A Real-Time Study of Homogeneous Nucleation, Growth, and Phase Transformations in Nanodroplets of Low Molecular Weight Isotactic Polypropylene Using AFM

Lekshmi Kailas,[†] Cvetelin Vasilev,[†] Jean-Nicolas Audinot,[‡] Henri-Noël Migeon,[‡] and Jamie K. Hobbs*,[†]

Departments of "Physics & Astronomy" and Chemistry, University of Sheffield, Sheffield S3 7RH, UK, and Département Science et Analyse des Matériaux CRPGL, 41 rue du Brill, L-4422 Belvaux, Luxembourg

Received April 12, 2007; Revised Manuscript Received July 20, 2007

ABSTRACT: Nanodroplets of isotactic polypropylene (iPP) were observed using temperature-controlled AFM in order to study the polymer's crystallization behavior. The nucleation, growth, and transformation of iPP crystals on heating have been directly imaged. The strong confinement of the polymer into nanoscale droplets has allowed the controlled observation of polymer nucleation as well as access to crystal growth at exceptionally high supercooling in iPP. Different modes of crystal growth were observed depending on the film thickness, including the formation of multiple independent homogeneous nuclei within single droplets. The temperature at which the onset of nucleation was observed in individual droplets was found to be dependent on the thickness as well as the volume of the droplets. For droplets with smaller thicknesses (<5 nm), the thickness of the droplets was found to be the dominating factor influencing the nucleation temperature. This is the first real-space, real-time observation of homogeneous nucleation in iPP, almost 125 °C below its melting point, which could signify crystal growth in the smectic form, and of the subsequent reorganization into the α-form.

Introduction

Despite its fundamental importance both to the theoretical understanding of polymer crystallization and to the industrial application of semicrystalline polymers, the process of crystal nucleation in polymeric systems remains infrequently studied and poorly understood due to the difficulty in observing the onset of a nucleation event. Crystallization is thought to occur via a two-step process of nucleation and crystal growth, although recent hypotheses suggest the involvement of many multistep processes during the initial stages of crystallization from a polymer melt, the possibility of an intermediate ordering process, and transient liquid phases preceding the final crystalline state.[1−3] The intermediate, partially ordered states that lie between the melt and final crystal phase are thought to play a crucial role in crystal growth.[4] Therefore, gaining new insights at the molecular level into the formation of the primary nucleus, its growth, and phase transformations is imperative in order to understand fully the mechanisms that govern crystallization. Here, we use the capability of atomic force microscopy (AFM) to obtain real-space, real-time images to shed further light on the processes of nucleation and crystal growth.

Isotactic polypropylene (iPP) is known to exhibit several crystalline polymorphs (monoclinic α-form, hexagonal *β*-form, orthorhombic *γ*-form), depending on the crystallization conditions and nucleating agents used; all having packing schemes based on a 3-fold helical conformation. Slow cooling from the melt is known to produce predominantly the α-modification; the usage of specific nucleating agents yields the *β*-form while elevated pressure and low degrees of supercooling results in the *γ*-phase.[5−15] The α-phase is found to be the more stable phase at atmospheric pressures.[16] On rapid quenching from the melt, it is also reported to reveal a mesomorphic or "smectic" phase, the exact nature and structure of which are still not fully known. It has been suggested that this metastable phase can be equated with the onset of homogeneous nucleation.[5]

There have been previous attempts to follow nucleation using AFM.[17−24] However, what is observed remains ambiguous because of the surface specific nature of the AFM technique—as the polymer film is relatively thick, it is not possible to say whether what is seen is a nucleation event or the growth of a crystal from a (subsurface) nucleus that crosses the sample surface. Secondary nucleation has been observed in several cases, both from lamellae[25−27] and from oriented "shish" structures.[18] In the case of rapidly crystallizing polymers such as iPP (and most other commercial polymers) the probability of observing the nucleation event in a bulk sample or thin film is vanishingly small. In most circumstances crystallization in a polymer melt is initiated by foreign particles. The aim of the current study is to follow homogeneous nucleation and subsequent crystal growth. To achieve this, we made use of the classical droplet method[28] in order to allow the formation of small volumes of highly supercooled melt, which are free from nucleating impurities. The idea is to break the sample up into a large number of spatially isolated droplets such that the number of droplets is greater than the number of active heterogeneities, so that homogeneous nucleation can be observed in some of these impurity-free droplets. AFM is utilized to directly image the nucleation process at the molecular scale.

Previous studies of polymer nucleation using the "droplet method" [29−32] have found that, once a sufficiently small droplet size is obtained, the rate of nucleation depends only on the supercooling and the droplet volume, in agreement with classical theories.[33] This is usually interpreted as strong evidence for homogeneous nucleation. In ref 31 it is argued convincingly that the observed behavior discounts the possibility of external interfaces of any kind (including a droplet's surface), causing or enhancing the nucleation rate over a range of length scales

* Corresponding author: Tel +44 114 222 9316; e-mail jamie.hobbs@sheffield.ac.uk.
[†] University of Sheffield.
[‡] CRPGL.

10.1021/ma070861t CCC: $37.00
Published on Web 09/07/2007

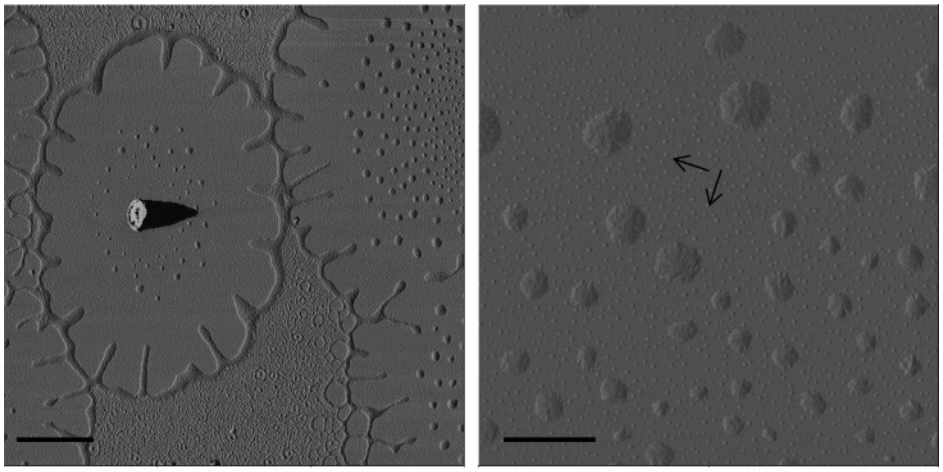

Figure 1. AFM phase images showing the dewetted iPP film on plasma-treated silicon substrate. (a) A classic dewetting pattern; scale bar represents 5 μm. (b) A closer view of the isolated iPP droplets; scale bar represents 1 μm. The arrows indicate small impurity spots. Black to white represents a change in phase of 70°.

from microns to just 10 nm under the experimental situation studied in those experiments (i.e., a dewetting surface). However, the question still remains as to what happens at smaller length scale, as the size scale of the droplet approaches or becomes smaller than the critical nucleus size in at least one dimension. Indeed, it is precisely in such confined geometries where nucleation has an enhanced effect, as the eventual crystal orientation will be strongly controlled by that of the nuclei as there is no opportunity, within the small confined volume, for the subsequent growth to introduce its usual dominance.

In this article we present AFM images of the onset of nucleation in iPP nanodroplets at high supercooling, the growth and ensuing morphology of the highly supercooled crystalline phase, and the phase transformation processes undergone by the iPP crystals on heating. Different modes of crystal growth were observed in these droplets depending on the film thickness as well as the volume of the droplets. In order to ascertain whether the nanodroplets were truly isolated, we made use of the depth profiling, chemical mapping technique of NanoSIMS.

Experimental Section

Low molecular weight iPP (M_w: 12 000; M_n: 5000) from Sigma-Aldrich was used as received. It was dissolved at a concentration of 1 mg/mL in *p*-xylene at 90 °C. The hot solution was dropped onto a silicon wafer (plasma treated for 30 min before being placed on the spin-coater), spinning at the rate of 5000 rpm for a time period of 30 s. The ultrathin film obtained (thickness <10 nm) was annealed for 10 min at 180 °C in a nitrogen atmosphere on a Linkam hot stage to allow dewetting into isolated droplets and then cooled to room temperature. This relatively low molecular weight sample was selected as it allowed the dewetting process to be adopted in order to create the nanodroplets—higher molecular weight material does not dewet sufficiently fast to avoid sample degradation. NanoSIMS was carried out on the sample to see whether the isolation was complete or whether there was a thin layer of the polymer connecting the various droplets. The dewetted iPP droplets obtained on annealing were examined at various temperatures after remelting at 180 °C in a nitrogen atmosphere, quenching the sample by transferring it to a hot stage preheated to 60 °C kept under the AFM scanner[18] and then slow cooling at about 0.3 °C/min from the melt while imaging with the AFM. A Peltier device kept in contact with the underside of the Linkam hot stage allows the lowering of temperature down to 0 °C.[34] The temperatures quoted are those displayed on the Linkam heater and are found to deviate from the actual sample surface temperature by less than a degree over the temperature range 20−40 °C.

Atomic force microscopy observations were carried out in air using a Digital Instruments D3100 AFM operated in Tapping Mode. Measurements were carried out using standard silicon cantilevers with a nominal spring constant of 50 N/m and resonant frequency of ~300 kHz. Height and phase data were collected simultaneously.

NanoSIMS experiments were performed using the Cameca NanoSIMS 50 in the raster imaging mode. The ionic images were obtained layer by layer using a beam of Cs^+ primary ions with an energy impact of 16 keV and a beam current of 0.8 pA on the sample (sputter rate ~ 10 nm/s). Negative secondary ion signals for $^{12}C^-$, $^{12}C^1H^-$, $^{16}O^-$, and $^{28}Si^-$ were collected simultaneously.

Results and Discussion

We focus our attention on isolated droplets formed on the silicon wafer by a dewetting mechanism in order to observe homogeneous nucleation and crystalline growth in small confined volumes. Figure 1a shows the AFM phase image of the iPP film which has undergone dewetting, in this case a nucleated dewetting process which helps to leave a final sample that is free from heterogeneities.[31] Larger impurities present in the sample tend to initiate nucleation and facilitate the dewetting of the film into flower-shaped holes. Inside the boundary of these holes, the dewetting film gives rise to hundreds of tiny droplets, many of which will be completely devoid of even tiny impurity particles, and these droplets are ideal sites for observing homogeneous nucleation. Figure 1b gives a closer view of the isolated iPP droplets on the surface of the plasma-treated silicon wafer, after annealing to 180 °C and then cooling to room temperature.

A range of polymer droplets of different sizes and shapes is apparent. As the dewetting process was not left to reach equilibrium, the droplet shape is highly flattened, with typical droplets measuring up to microns in diameter but still only a few nanometers in height above the substrate. It is evident from Figure 2 (NanoSIMS image) that these droplets are essentially isolated. The SiO_x layer on the substrate is responsible for the high-intensity ^{16}O signal coming from the medium surrounding the droplets, indicating that there is no interconnecting layer of polymer between the droplets.

In Figure 1b the presence of a population of very small spots evenly distributed throughout the sample surface is apparent (arrowed), the nature of which is unclear. As the size of these spots are lower than the 50 nm lateral resolution of NanoSIMS, no conclusive evidence can be drawn from the NanoSIMS data

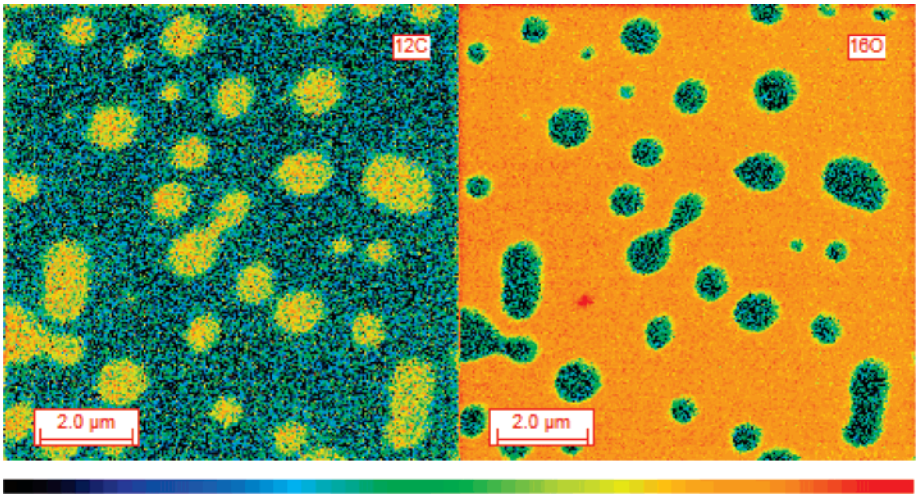

Figure 2. NanoSIMS images of the outermost surface layer. The image on the left shows ^{12}C signal while that on the right shows ^{16}O signal. The color bar from black to red signifies increasing signal intensity.

regarding the chemical composition of these spots. However, as they do not change throughout our experiments, and do not appear to interfere with or initiate crystal growth, we assume them to be either lower molecular weight fragments of poor tacticity or, more probably, non-nucleating impurities possibly inherent in the commercial sample.

The melting temperature of this polymer is 157 °C as measured from DSC data. The polymer was remelted at 180 °C so that the sample would be devoid of any crystal nuclei that could initiate crystallization. After quenching it and cooling slowly from 60 °C, in-situ AFM studies were carried out to track the changes undergone by the various droplets on the sample surface. A series of experiments were conducted on similar samples prepared under similar conditions.

From these experiments, we were able to observe three different types of nucleation behavior and crystal growth patterns in the dewetted droplets. The most common behavior observed was that of instantaneous nucleation and crystal growth in isolated droplets, where the rate of growth was too rapid for the conventional AFM to follow, such that we obtained images of a molten droplet in one frame which had crystallized entirely by the time the next frame was imaged. Apart from this rapid crystal growth behavior, we were also able to observe slow crystal growth initiated by two distinguishable nucleation methods—one by the formation of a single nucleus in an isolated droplet and the other by the formation of multiple nuclei inside one droplet. Detailed interpretations of AFM images and possible explanations for these different behavior patterns are given below.

Figure 3 gives a series of AFM phase images which show the "classical" instantaneous nucleation and rapid crystal growth behavior while the sample was cooled from 60 °C. In these phase images, the amorphous areas appear as darker and the crystallized ones as brighter areas, with the silicon having a similar phase contrast to the crystalline polymer. Artifacts like the white rims around the droplets in Figure 3 appear in phase images as these images are influenced by the surface topography at sharp edges, steps, etc., where the error in the feedback loop is large. The white arrows in Figure 3a show the position of the droplets still in the molten state. The white arrows in the subsequent images show the position of these droplets which have subsequently undergone crystallization. The droplets are found to have thicknesses in the range 5−10 nm.

Figure 4 shows the AFM phase images of the nucleation from a single nucleus and crystalline growth within one of the droplets (diameter of ∼700 nm) on cooling at the rate of 0.3 °C/min. On reaching a temperature of 34.8 °C, nucleation is detected (Figure 4b). At 33.6 °C, the nucleus is seen to have grown to have a crystal morphology that is neither cross-hatched nor granular but probably best described as axialitic (Figure 4c). As AFM is a serial technique, with images being collected line by line through a continuous raster scanning of the surface, it is possible to misinterpret the sequence of events shown in a series of images. In this case all images were collected while scanning from the top to the bottom. So, the lower, amorphous, section of the droplet in Figure 4b was imaged by the AFM tip after the upper section of the droplet containing the nucleus had been scanned. Therefore, the growth of the crystal shown in Figure 4c was not instantaneous but did in fact grow from the nucleus in Figure 4b at a rate that was slower than the "slow-scan" velocity of the AFM tip. The droplet is very thin (∼2 nm as measured by AFM), so it is highly unlikely that there are any heterogeneities within the droplet to cause nucleation as these would be imaged by the AFM. The only possible nucleating "agent" is the substrate itself. Also, there is no possibility of significant growth having occurred below the surface imaged, as any hard object larger than a few nanometers would be seen. We therefore suggest that the crystalline object seen in Figure 4b is the primary nucleus having dimensions of 120 × 50 nm, captured soon after reaching critical size, and that this nucleus has formed homogeneously. Studies on natural rubber imply that the homogeneous nucleus can be no longer than the lamellar thickness.[35] Therefore, the critical size is most probably substantially smaller than the dimensions mentioned above—our measurement gives an upper bound. Further cooling shows no change in the crystal size or shape, as seen from Figure 4d,e.

We can estimate a maximum possible growth rate of the iPP at this temperature from these images, as the distance from the nuclei to the lowermost point of the structure (Figure 4c) divided by the time for the 20 scan lines of the image to be taken when this point was first past in Figure 4b. This estimation is complicated by the fact that AFM is a serial technique, the image being collected line by line. Although the crystal growth might have taken longer to reach this point, it cannot have got there faster than this rate, as in that case the growing crystal would have overtaken the scanning tip and we would have seen it in the image. This calculation gives 40 nm s^{-1} as the maximum possible growth rate at this temperature in a ∼2 nm thick film, with 1.7 nm s^{-1} as the minimum possible rate (i.e., the distance

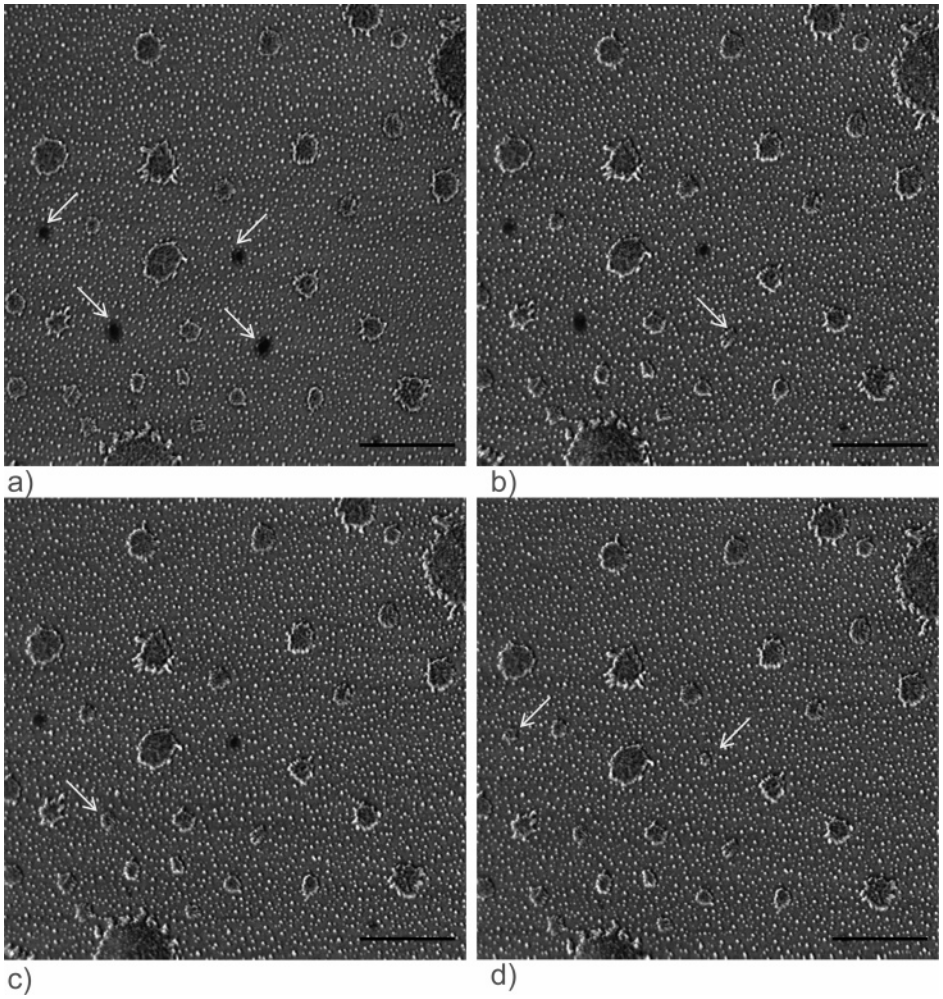

Figure 3. A series of AFM phase images showing instantaneous nucleation and crystal growth. The color scale black to white represents a change in phase of 50°, and the scale bar represents 1 μm. The white rims to the droplets are an imaging artifact (see text). The images were taken at (a) 40, (b) 38, (c) 37.5, and (d) 37 °C.

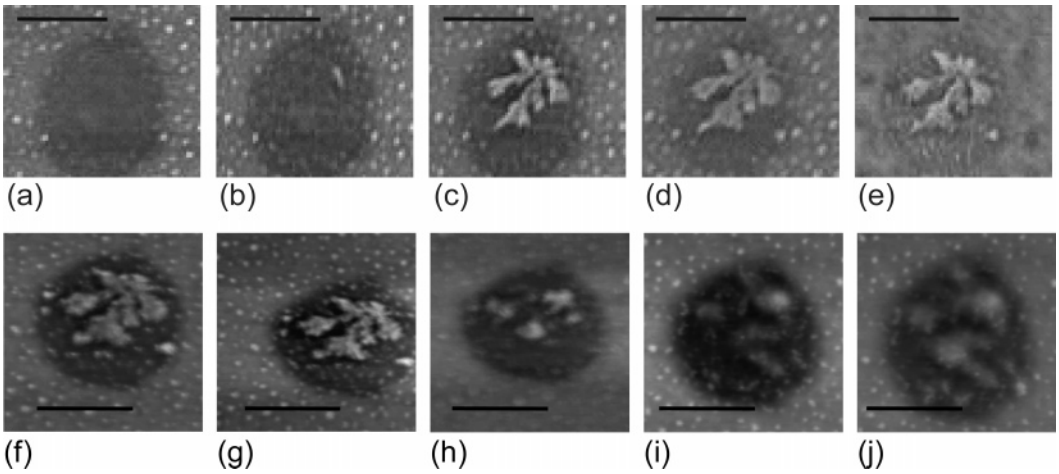

Figure 4. A series of AFM phase images showing the crystallization on cooling (top row) and reorganization on heating (bottom row) of an iPP droplet. Black to white represents a change in phase of 50° (a−e) and 80° (f−j), and the scale bar represents 500 nm. (a) Taken at 40, (b) 34.8, (c) 33.6, (d) 23.2, (e) 15, (f) 60, (g) 80, (h) 90, (i) 97, and (j) 102 °C.

grown/the time interval between two consecutive scans). The relatively slow growth rate as opposed to the rapid growth rate implied in ref 36 is most probably due to the high level of confinement experienced by the very thin droplet. At these high supercoolings, close to the glass transition temperature, the rate of material transport in such a thin film must considerably reduce the crystal growth rate.

As seen in these images, even on cooling the sample, some of the iPP in the droplets is left uncrystallized (the darker background that retains the original droplet shape); it is probable that there is some lower molecular weight and low tacticity component of the sample that is effectively noncrystallizable. These could be excluded from the growing crystal, and this exclusion process would be expected to reduce the growth rate.

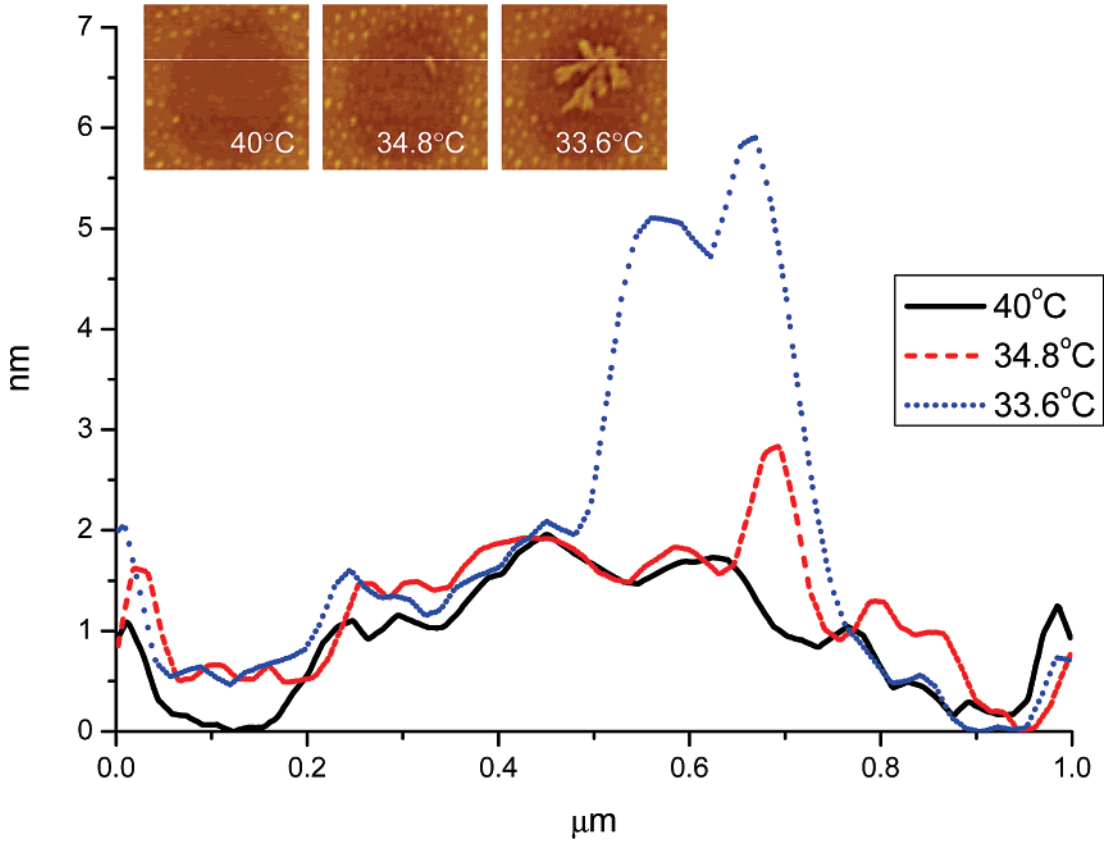

Figure 5. Comparison between the line profiles of the iPP droplet shown in Figure 4 taken at 40, 34.8, and 33.6 °C.

Most probably, the slow growth rate seen is due to a combination of sample purity and film thickness effects. Considering the behavior of the other (thicker) droplets such as those in Figure 3, we suggest film thickness to be the dominant factor in this case.

Section profiles of the droplet shown in Figure 4 were taken and are given in Figure 5. The height of the molten droplet shown in Figure 4a was found to be ∼2 nm. The initial nucleus in Figure 4b was found to have a thickness of ∼2.8 nm. The section profile shows that by the time the crystalline growth has developed to the shape shown in Figure 4c, it has a height of ∼5.8 nm. The initial, as nucleated, crystal thickness is surprisingly thin and rapidly thickens between images to the final thickness that it then maintains. Such thickening growth at these high supercoolings is indicative of substantial mobility within the crystalline phase, supporting the suggestion, discussed in the next section, that crystal growth is in the smectic phase.

Previous studies at comparable supercoolings have found that iPP crystallizes in the smectic phase.[8,37,38] Here, we have used the in-situ capabilities of the AFM to image the same area on heating. Figure 4f−j show a series of phase images taken on heating the sample from 60 to 105 °C, tracking the crystalline structure inside the droplet. The slight distortion in the droplet size could be attributed to the mechanical changes associated with scanning at higher temperatures. The fact that the background appears darker on reheating most probably occurs as there are changes in the physical properties of the polymer with an increase in temperature (i.e., it becomes softer and more sticky). From the AFM images, it appears that the crystal, initially formed at 33.6 °C (Figure 4c), remains unaltered even on heating to 80 °C (Figure 4g). But the image taken at 90 °C (Figure 4h) shows that the structure has disintegrated and at 97 °C (Figure 4i) there is the emergence of a rearranged crystalline form. Wang et al.[8] using WAXD have shown that the phase transformation from the mesomorphic into a crystalline phase occurs at temperatures above 80 °C. Hsu et al.[39] using DSC also showed a smectic to monoclinic transformation at ca. 80 °C. This is in accord with our AFM measurements which show the crystalline structure formed at a lower temperature of 34.8 °C, disintegrating between 80 and 90 °C and rearranging itself into a different conformation. This is not unequivocal evidence that the structure is in the smectic phase—α-phase crystals formed at such low temperatures would most probably reorganize on heating. However, as the change in morphology is very significant, with a complete change in the morphology during the rearrangement, and as the onset of homogeneous nucleation is also inferred to correspond with the formation of the mesomorphic phase,[5] it is highly probable that the primary nucleus formed at 34.8 °C and which completed its growth at lower temperatures is the "smectic" form of iPP. Previous images of smectic iPP[8,39,40] have shown a course, granular texture, while in our images we see a clear crystal form. It is possible that the difference in morphology is due to the constrained nature of the growth in the system studied here, preventing in-filling that usually hides the original form.

The third form of nucleation—sporadic nucleation in droplets that does not then lead to substantial growth, with further nucleation occurring later in the same droplet—is the most unexpected. Figure 6 shows a series of images showing this mode of growth. In order to interpret the images more easily, white circles are used to indicate the droplets under investigation; black arrows indicate the onset of nucleation.

In Figure 6b,c the commencement of crystalline growth is observed in two of the droplets (indicated by the black arrows). In Figure 6e,f the appearance of crystal nuclei wholly unconnected from the previously crystallized areas in the same droplets can be seen. These crystal nuclei are formed at very high supercooling, even higher than those which resulted in crystal-

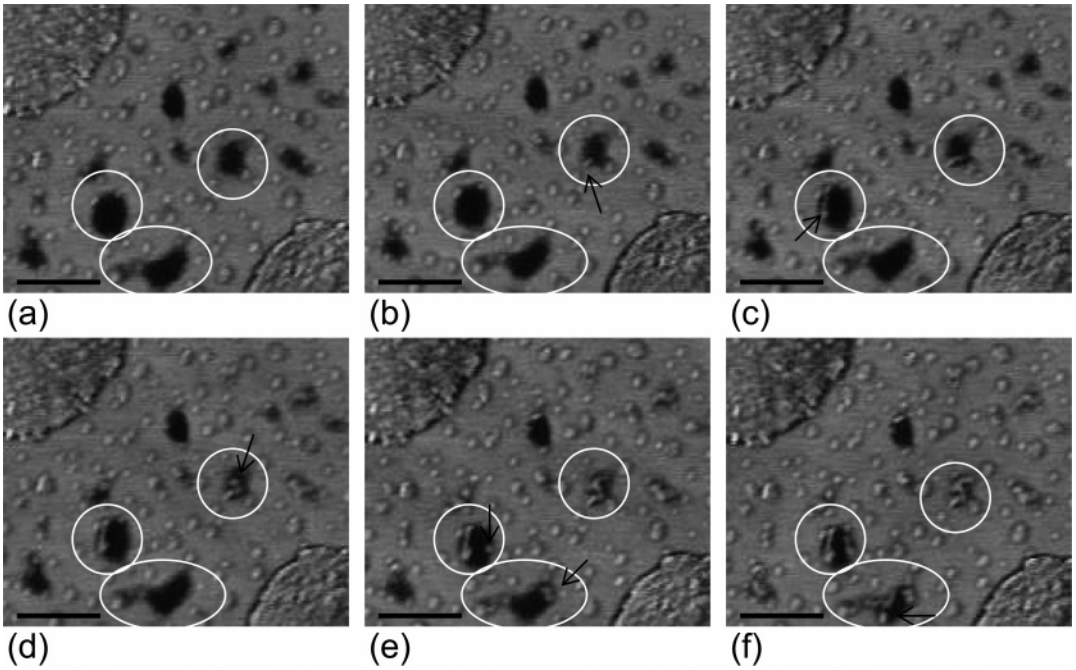

Figure 6. A series of AFM phase images showing the slow crystallization in iPP droplets. Black to white represents a change in phase of 30°, and the scale bar represents 200 nm. (a) Taken at 35.8, (b) 33, (c) 32, (d) 31.5, (e) 30, and (f) 29.5 °C. The white circles indicate the droplets under investigation, and the black arrows indicate when a new nucleus initiates growth.

lization from a single nucleus (shown in Figure 4). The images clearly show that instead of one single nucleus initiating growth inside the droplet, there is more than one nucleus, appearing at different times which slowly grow and fill the entire droplet. The growth of these crystals is at such a very slow rate that we were able to track the formation of the various nuclei as well as the lamellar growth. The fact that these nanodroplets support multiple sites of initial nucleation and the extremely slow growth rate make this type of crystal growth behavior very peculiar. There are several possible explanations. It may be that, because of the very thin film thickness, growth following the initial nucleation event is severely hindered by the depletion of crystallizable material that occurs during nucleation, with subsequent transport over the surface being too slow at this temperature relatively close to the glass transition temperature. So, nucleation has an opportunity to be initiated in other sites within the droplet, before it has been completely crystallized by the growth that has started from one nucleus. Alternatively, if we assume growth is in the mesomorphic phase at these high supercoolings, it is possible that this highly defective phase grows very slowly—although this seems unlikely as it supplies no explanation for the slow growth seen in these thin films compared to the almost instantaneous growth observed in macroscopic samples. It may be that the polymer chains adjacent to the surface are pinned in some way and hence have reduced mobility, leading to slow growth. However, this seems rather unlikely, considering the fact that this surface dewets at high temperatures and leaves no polymer behind, implying minimal attractive interaction between the polymer and the surface. Another possibility is that there is an orientational effect—if the initial nucleus is oriented such that the fast growth direction is perpendicular to the surface, it cannot grow very rapidly (or at all for certain possible orientations), so the geometric effect of confinement heavily slows growth and allows time for multiple nucleation. Indeed, as the films are so thin it seems unlikely (though not impossible) that the chains will orient perpendicular to the substrate in all cases, the orientation that would be most efficient for subsequent thin film growth. From the data obtained it is impossible to make a definitive selection from these (or other) possibilities, although the last seems the most likely explanation.

AFM not only allows the crystallization process to be imaged but also provides an opportunity to measure directly the volume of crystallizable material and to provide some test of nucleation theory. Data were collected from droplets having thickness ranging from 0.5 to 6 nm and volumes from 4800 to 700 000 nm^3 (taken from six different samples analyzed on different days, but all made using the same sample preparation technique). We utilized Veeco Nanoscope software in order to measure the thickness and Image SXM[41] to compute the volume of each individual droplet. On analyzing the data, we found that the rapid growth occurred in droplets having a thickness ~5 nm and higher as well as volume greater than 700 000 nm^3. Single nucleus formation and growth was found in highly flattened droplets of around 2−3 nm height and volumes less than those which exhibited the rapid growth. Droplets with thicknesses between 5 and 3.5 nm and volume less than 100 000 nm^3 exhibited the formation of multiple nuclei inside the same droplet.

Figure 7a shows the graph of the crystallization temperature vs the volume of the droplets while Figure 7b gives the plot of the temperature against the thickness of the droplets. The temperature plotted is the one at which the onset of nucleation is detected (as in some droplets which produced more than one nucleation site, nucleation occurred over several degrees). Ideally, data would have been collected at a series of fixed temperatures and the rate dependence of nucleation measured at each temperature for different droplet populations. Unfortunately, the relatively limited "field of view" of the AFM while maintaining high resolution, as well as the difficulty of imaging stably for such extended periods, made such an experiment impossible, despite numerous attempts. However, data of the form obtained still provide useful information for comparison with theory. If nucleation is truly random in space (i.e., independent of interfaces), the rate (i.e., number of nuclei per unit volume per unit time) would vary very strongly with volume

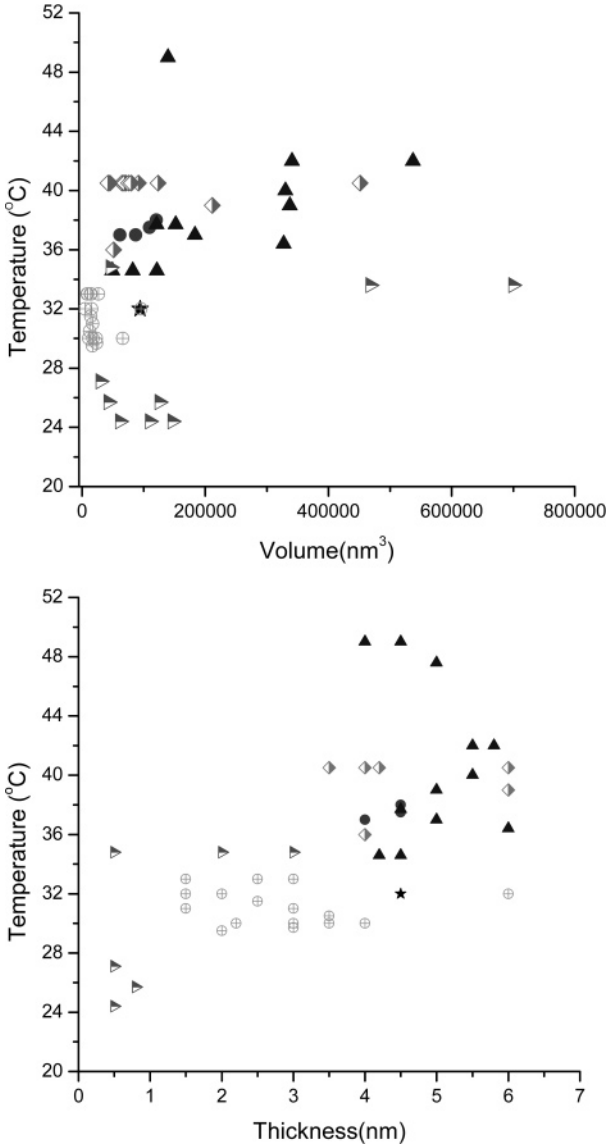

Figure 7. (a) Plot of the crystallization temperature vs the volume of the droplets and (b) plot of the crystallization temperature vs the thickness of the droplets obtained from six samples (shown in the graph using six different symbols).

and little with thickness. Alternatively, a stronger variation with thickness implies either a surface effect or some other confinement effect.

From the graphs, it is clear that the crystallization temperature increased with the thickness as well as the volume of the droplets. Previous experiments have also shown that larger droplets nucleate faster than smaller ones, owing to a higher probability of nucleation in a bigger volume.[31] From Figure 7a there is a notable influence of volume on the nucleation temperature for droplets with larger volumes. For smaller volumes, the curve is essentially vertical, indicating that the nucleation temperature is independent of the volume in this range. From Figure 7b, it is seen that the nucleation temperature vs thickness curve is linear for the entire data set, although very scattered. So it can be concluded that for the smallest thicknesses (<5 nm) the thickness of the droplets becomes the dominating factor which influences the nucleation temperature, with essentially no effect of volume. At larger thicknesses, volume also starts to have an influence. To define which is the dominant factor in the thicker film case would require considerably more data, going to larger volumes and thicknesses (and hence temperatures). However, we can define this thickness as the point of a transition in behavior, in that volume is now having an effect—whether thickness also continues to have a strong influence at greater thicknesses or whether its apparent continuing effect is due to the coupling between thickness and volume in the population of (pancake-shaped) droplets measured is unclear. In ref 32, the authors, on investigating small volumes, found that the nucleation still had a dependence on the droplet volume in systems down to ~10 polymer chains and was not influenced by the interface. In that work the thinnest droplets studied were greater than 5 nm in thickness. From the examination of our data (Figure 7) it appears that the "transition" in behavior occurs at a thickness slightly smaller than that encountered in ref 32. It is possible that this change occurs because the dimension of the critical nucleus is now comparable to the film thickness. The α-phase unit cell parameters have been found to be $a = 6.65 \pm 0.05$ Å, $b = 20.96 \pm 0.15$ Å, $c = 6.50 \pm 0.05$ Å, $\alpha = \gamma = 90°$, and $\beta = 99.6°$.[42,43] The chain axis repeat is 6.5 Å. In these very thin films the number of unit cell repeat distances available within the initial film thickness is very limited. Once the critical nucleus size in at least one dimension is comparable to the film thickness the rate of nucleation is likely to drop, as nucleation requires a fluctuation which includes an increase in height of the droplet. We therefore suggest that this is a thickness, rather than a surface, effect.

Conclusions

We have imaged in-situ, in real space, for the first time, the nucleation and growth of iPP crystals at a supercooling of more than 125 °C using AFM. Homogeneous nucleation has been unambiguously observed. By following the subsequent reorganization of the structure on heating, we suggest that the crystals formed are in the mesomorphic form. Direct, real-space observation of crystallization in the mesomorphic form shows the development of a clear crystal morphology. Real-time imaging of these crystals during heating shows a complete rearrangement of the structure as expected, given the considerable amount of chain reorganization that is necessary between the statistical up−down chain alignment in the mesomorphic and the antiparallel chain packing in the α-phases.

The thicknesses of the droplets as well as their volume have been found to have an influence on the temperature at which nucleation is initiated as well as the mode of crystal growth. For smaller thicknesses (<5 nm), we have found that the nucleation temperature depends on the thickness of the droplets.

The formation of isolated droplets with nanometric dimensions provides a powerful tool for in-situ observation of nucleation processes and of crystallization at very high supercoolings in materials that, in bulk samples, cannot be deeply quenched. Combination with temperature controlled AFM allows these nonequilibrium processes to be followed in-situ, in real time, with nanometer resolution.

Acknowledgment. L. Kailas, C. Vasilev, and J. K. Hobbs thank the EPSRC, UK, for funding. We also thank Mr. O. Farrance (Dept. of Physics & Astronomy, University of Sheffield) for the development of the low-temperature system and temperature calibration. The NanoSIMS analyses have been performed with the financial support from Fond National de la Recherche of Luxembourg.

References and Notes

(1) Strobl, G. *Eur. Phys. J. E* **2000**, *3*, 165.

(2) Olmsted, P. D.; Poon, W. C. K.; McLeish, T. C. B.; Terrill, N. J.; Ryan, A. J. *Phys. Rev. Lett.* **1998**, *81*, 373.
(3) Heeley, E. L.; Maidens, A. V.; Olmsted, P. D.; Bras, W.; Dolbnya, I. P.; Fairclough, J. P. A.; Terrill, N. J.; Ryan, A. J. *Macromolecules* **2003**, *36*, 3656.
(4) Keller, A.; Hikosaka, M.; Rastogi, S.; Toda, A.; Barham, P. J.; Goldbeck-wood, G. *J. Mater. Sci.* **1994**, *29*, 2579.
(5) Lotz, B. *Acad. Nazionale Lincei* **2004**, 107.
(6) Lotz, B.; Wittmann, J. C.; Lovinger, A. J. *Polymer* **1996**, *37*, 4979.
(7) Meille, S. V.; Bruckner, S.; Porzio, W. *Macromolecules* **1990**, *23*, 4114.
(8) Wang, Z.-G.; Hsiao, B. S.; Srinivas, S.; Brown, G. M.; Tsou, A. H.; Chang, S. Z. D.; Stein, R. S. *Polymer* **2001**, *42*, 7561.
(9) Nedkov, E.; Dobreva, T. *e-Polym.* **2002**, *042*, 1.
(10) Merajver, S. D.; Wunder, S. L.; Wallace, W. *J. Polym. Sci., Polym. Phys.* **1985**, *23*, 2043.
(11) Tordjeman, Ph.; Robert, C.; Marin, G.; Gerard, P. *Eur. Phys. J. E* **2001**, *4*, 459.
(12) Fillon, B.; Lotz, B.; Thierry, A.; Wittmann, J. C. *J. Polym. Sci., Part B: Polym. Phys.* **1993**, *31*, 1395.
(13) Stocker, W.; Schumacher, M.; Graff, S.; Thierry, A.; Wittmann, J. C.; Lotz, B. *Macromolecules* **1998**, *31*, 807.
(14) Mezghani, K.; Phillips, P. J. *Polymer* **1997**, *38*, 5725.
(15) Mezghani, K.; Phillips, P. J. *Polymer* **1998**, *39*, 3735.
(16) Dimeska, A.; Phillips, P. J. *Polymer* **2006**, *47*, 5445.
(17) Massa, M. V.; Dalnoki-Veress, K.; Forrest, J. A. *Eur. Phys. J. E* **2003**, *11*, 191.
(18) Hobbs, J. K.; Humphris, A. D. L.; Miles, M. J. *Macromolecules* **2001**, *34*, 5508.
(19) Hobbs, J. K. *Chin. J. Polym. Sci.* **2003**, *21*, 135.
(20) Lei, Y.-G.; Chan, C.-M.; Li, J.-X.; Ng, K.-M.; Wang, Y.; Jiang, Y.; Li, L. *Macromolecules* **2002**, *35*, 6751.
(21) Pearce, R.; Vansco, G. J. *Macromolecules* **1997**, *30*, 5843.
(22) Li, L.; Chan, C.-M.; Li, J.-X.; Ng, K.-M.; Yeung, K.-L.; Weng, L.-T. *Macromolecules* **1999**, *32*, 8240.
(23) Li, L.; Chan, C.-M.; Yeung, K.-L.; Li, J.-X.; Ng, K.-M.; Lei, Y. *Macromolecules* **2001**, *34*, 316.
(24) Beekmans, L. G. M.; Vancso, G. J. *Polymer* **2000**, *41*, 8975.
(25) Chen, E.-Q.; Jing, A. J.; Weng, X.; Huang, P.; Lee, S.-W.; Cheng, S. Z. D.; Hsiao, B. S.; Yeh, F. *Polymer* **2003**, *44*, 6051.
(26) Lei, Y.-G.; Chan, C.-M.; Wang, Y.; Ng, K.-M.; Jiang, Y.; Lin, L. *Polymer* **2003**, *44*, 4673.
(27) Hobbs, J. K.; McMaster, T. J.; Miles, M. J.; Barham, P. J. *Polymer* **1998**, *39*, 2437.
(28) Vonnegut, B. *J. Colloid Sci.* **1948**, *3*, 563.
(29) Taden, A.; Landfester, K. *Macromolecules* **2003**, *36*, 4037.
(30) Tol, R. T.; Mathot, V. B. F.; Groeninckx, G. *Polymer* **2005**, *46*, 2955.
(31) Massa, M. V.; Dalnoki-Veress, K.; *Phys. Rev. Lett.* **2004**, *92*, 255509.
(32) Massa, M. V.; Carvalho, J. L.; Dalnoki-Veress, K. *Phys. Rev. Lett.* **2006**, *97*, 247802.
(33) Strobl, G. *The Physics of Polymers;* 2nd ed.; Springer-Verlag: Berlin, 1997.
(34) Hobbs, J. K.; Humphris, A. D. L.; Miles, M. J. *ACS Symp. Ser.* **2005**, *897*, 194.
(35) Edwards, B. C.; Phillips, P. J. *J. Polym. Sci., Polym. Phys. Ed.* **1975**, *13*, 2117.
(36) Gradys, A.; Sajkiewicz, P.; Minakov, A. A.; Adamovsky, S.; Schick, C.; Hashimoto, T.; Saijo, K. *Mater. Sci. Eng., A* **2005**, *413*−*414*, 442.
(37) Jin, Y.; Hiltner, A.; Baer, E.; Masirek, R.; Piorkowska, E.; Galeski, A. *J. Polym. Sci., Part B: Polym. Phys.* **2006**, *44*, 1795.
(38) Uriguen, J. I.; Bremer, L.; Mathot, V.; Groeninckx, G. *Polymer* **2004**, *45*, 5961.
(39) Hsu, C. C.; Geil, P. H.; Miyaji, H.; Asai, K. *J. Polym. Sci., Part B: Polym. Phys.* **1986**, *24*, 2379.
(40) Gezovich, D. M.; Geil, P. H. *Polym. Eng. Sci.* **1968**, *8*, 202.
(41) Barrett, S. D. Image SXM 2007, http://www.ImageSXM.org.uk.
(42) Natta, G.; Corradini, P. *Nuovo Cimento Suppl.* **1960**, *15*, 40.
(43) Bruckner, S.; Meille, S. V.; Petraccone, V.; Pirozzi, B. *Prog. Polym. Sci.* **1991**, *16*, 361.

MA070861T